PHYSICAL REVIEW D **93,** 043531 (2016)

Searching for scalar gravitational interactions in current and future cosmological data

Alireza Hojjati,[1,2] Aaron Plahn,[2] Alex Zucca,[2] Levon Pogosian,[2] Philippe Brax,[3] Anne-Christine Davis,[4] and Gong-Bo Zhao[5,6]

[1]*Department of Physics and Astronomy, University of British Columbia, Vancouver, British Columbia V6T 1Z1, Canada*
[2]*Department of Physics, Simon Fraser University, Burnaby, British Columbia V5A 1S6, Canada*
[3]*Institut de Physique Theorique, CEA, IPhT, CNRS, URA 2306, F-91191Gif/Yvette Cedex, France*
[4]*DAMTP, Centre for Mathematical Sciences, University of Cambridge, Wilberforce Road, Cambridge CB3 0WA, United Kingdom*
[5]*National Astronomy Observatories, Chinese Academy of Science, Beijing 100012, People's Republic of China*
[6]*Institute of Cosmology and Gravitation, University of Portsmouth, Portsmouth PO1 3FX, United Kingdom*

(Received 25 November 2015; published 17 February 2016)

Modified gravity theories often contain a scalar field of gravitational strength which interacts with matter. We examine constraints on the range and the coupling strength of a scalar gravitational degree of freedom using a subset of current data that can be safely analyzed within the linear perturbation theory. Using a model-independent implementation of scalar-tensor theories in MGCAMB in terms of two functions of the scale factor describing the mass and the coupling of the scalar degree of freedom, we derive constraints on the $f(R)$, generalized chameleon, symmetron and dilaton models. Since most of the large scale structure data available today is from relatively low redshifts, only a limited range of observed scales is in the linear regime, leading to relatively weak constraints. We then perform a forecast for a future large scale structure survey, such as the Large Synoptic Survey Telescope (LSST), which will map a significant volume at higher redshifts, and show that it will produce much stronger constraints on scalar interactions in specific models. We also perform a principal component analysis and find that future surveys should be able to provide tight constraints on several eigenmodes of the scalar mass evolution.

DOI: 10.1103/PhysRevD.93.043531

I. INTRODUCTION

A nonvanishing cosmological constant, Λ, is the simplest and the most common explanation of the observed cosmic acceleration [1,2]. Because, gravitationally, Λ is equivalent to the large vacuum energy predicted in particle physics, its value requires a technically unnatural fine-tuning [3,4] in order to be consistent with observations. The cosmological constant could be embedded in a larger class of dark energy models, where dynamics dictate the value of the vacuum energy. Because of the absence of apparent violation of Lorentz invariance in the Universe, dark energy is commonly described by the field theory of a scalar. Usually, some degree of fine-tuning of the parameters of the model must be introduced.

Another explanation could be provided by a modification of the laws of gravity on large scales. Such modifications generically involve a scalar degree of freedom which can lead to dynamical dark energy when the range of the scalar interaction is cosmological. As a result, scalar-tensor models with couplings to matter represent a well-motivated and versatile class of dark energy. Theories describing the behavior of the scalar field involve conformal [5] and disformal couplings to matter [6,7]. It turns out that the disformal coupling is severely constrained by local experiments and cosmological observations [8,9]. On the other hand, the conformal couplings, albeit large on cosmological scales, can be screened in the local environment where none of their effects, such as deviations from Newton's law, have been uncovered.

In this paper, we will focus on scalar-tensor models with screening mechanisms that are broadly classified to be of chameleon type [10,11], i.e. where either the mass of the scalar and/or its coupling to matter has a dependence of the local matter density. Specifically, we will consider three types of models with the chameleon property: the $f(R)$ theories [12,13], the environmentally dependent dilaton [14] and the symmetron [15]. The latter two models use the Damour-Polyakov mechanism for screening [16]. We will take advantage of the fact that these three very different types of models can be described using the same formalism defined in terms of two dynamical functions $m(a)$ and $\beta(a)$, where a is the scale factor [17,18]. The first one represents the mass of the scalar in the cosmological background at the redshift $1+z=a^{-1}$ and the second one is the coupling of the scalar to matter. The growth of cosmological perturbations in these models in the linear

regime and on subhorizon scales can be entirely described using a single function, $\epsilon(k,a) = 2\beta^2(a)/[1 + m^2(a)a^2/k^2]$, which appears in the modification of Newton's constant and in the modified relation between the curvature and the gravitational potential. While in this paper we shall restrict ourselves to observables which are sensitive to the linear regime only, we note that, given $m(a)$ and $\beta(a)$, one can also reconstruct the full nonlinear dynamics of the models. Namely, using a known evolution of the background matter density, $\rho(a)$, one can express the mass and the coupling as functions of local matter density: $m(\rho(x,t))$ and $\beta(\rho(x,t))$ and use them to perform N-body simulations of these models or to analyze local gravitational tests.

Modified gravity (MG) and its comparison with dark energy has been investigated using various cosmological probes in the last ten years [19–44]. Some models of modified gravity, such as the $f(R)$ theories, have been strongly constrained by observations both cosmological and astrophysical. The strongest bound on the range of the scalar interaction, expressed in terms of the parameter f_{R_0}, is at the level of 10^{-7} and comes from astrophysical tests of modified gravity using the period of Cepheids or the gas dynamics of dwarf galaxies [45–47]. The cosmological bounds are less effective, at the level of 10^{-5} [43,48]. On the other hand, dilatons and symmetrons have not been constrained as systematically as $f(R)$ on cosmological scales. Only a few tests have been performed using the $[m(a),\beta(a)]$ parametrization [42]. The strongest bounds on dilatons and symmetrons still spring from local gravitational tests [49]. Local tests of gravity for the chameleon-type models of modified gravity imply that the range of the scalar interaction cannot exceed 1 Mpc, implying that linear analyses are limited to probing only some of the features of the chameleon screening mechanisms. On the other hand, studying effects of modified gravity on shorter scales requires the use of either semianalytical methods suited to the quasilinear regime of cosmological perturbations or N-body simulations, both of which are model specific. Here, in order to keep our analysis as model independent as possible, we shall restrict ourselves to observables which are sensitive to the linear regime only.

The range of scales that are safely in the linear regime at low redshifts is quite limited. Most of the large scale structure data available today are from relatively low redshifts and provide only weak constraints on scalar-tensor models unless one considers information from nonlinear scales. The only way to do so is to run N-body simulations for specific models. On the other hand, future surveys, such as LSST [50] and Euclid [51], will provide a high volume of data from higher redshifts at which the range of linear scales is significantly larger, allowing one to deduce stronger constraints on scalar interactions not only for specific models but in a more general model-independent way. In this paper, we start by deriving constraints on $f(R)$, symmetron and dilaton models from the subset of today's data that can be safely considered to be in the linear regime. Then we perform a Fisher forecast for the same models assuming data from a future LSST-like survey in combination with other types of data expected over the next 5–10 years to show that they will be significantly tighter. Finally, we perform a principal component analysis (PCA) forecast of $m(a)$ for the same future data, assuming that $\beta(a)$ is a slowly varying function that can be taken to be a $\mathcal{O}(1)$ constant over the range of redshifts relevant to LSST.

While some our analysis can be compared to that in previous works, including [44], it is different and new in several ways. We consider specific scalar-tensor models (generalized chameleon, symmetron and dilaton) in a general framework, with the $[m(a),\beta(a)]$ parametrization, using all the available data on the linear scales. We use the widely studied and familiar Hu-Sawicki *f(R)* model to investigate in detail the degeneracy with neutrino masses and the lensing amplitude A_L and provide a physical interpretation for the observed effects. We find the current constraints on parameters of our general framework and use them as a baseline for comparison with the forecasted results. Finally, the discretized treatment of $[m(a),\beta(a)]$ parametrization and the PCA analysis provide a model-independent estimation of the capabilities of future surveys in constraining the scalar-tensor models of gravity.

II. THE MODEL

We consider scalar-tensor theories defined by the action

$$S = \int d^4x\sqrt{-g}\left[\frac{R}{16\pi G} + L_\phi + L_m[\psi, A^2(\phi)g_{\mu\nu}]\right], \quad (1)$$

where $g_{\mu\nu}$ is the Einstein frame metric, ψ are the matter fields that follow geodesics of $A^2(\phi)g_{\mu\nu}$, and L_ϕ is the scalar field Lagrangian given by

$$L_\phi = -\frac{(\partial\phi)^2}{2} - V(\phi). \quad (2)$$

The action in Eq. (1) is a generalized Brans-Dicke (GBD) theory [5] that includes a potential for the scalar field. In all GBD, the scalar field mediates an additional gravitational interaction between massive particles. The net force on a test mass is given by

$$\vec{f} = -\vec{\nabla}\Psi - \frac{d\ln A(\phi)}{d\phi}\vec{\nabla}\phi, \quad (3)$$

where Ψ is the Newtonian potential. Since solar system and laboratory tests severely constrain the presence of the scalar force, GBD can only be viable if either the coupling of the scalar field to matter is always negligible, or if there is a dynamical screening mechanism that suppresses the force in dense environments. The latter can be accomplished with appropriately chosen functional forms of $A(\phi)$ and $V(\phi)$.

Because of its coupling to matter, the scalar field dynamics are determined by an effective potential which takes into account the presence of the conserved matter density ρ of the environment

$$V_{\rm eff}(\phi) = V(\phi) + (A(\phi) - 1)\rho. \tag{4}$$

For some forms of $V(\phi)$ and $A(\phi)$, the effective potential can have a density-dependent minimum, $\phi(\rho)$. The scalar force will be screened if either the mass of the field happens to be extremely large or the coupling happens to be negligibly small at the minimum of $V_{\rm eff}(\phi)$. Such models can be broadly classified as "generalized chameleons" (GC), and include the original chameleon model [10], $f(R)$, dilatons [14] and symmetrons [15].

We note that the GC scalar-tensor theories considered in this work are viable only if the field stays at the minimum of the effective potential $V_{\rm eff}(\phi)$ [18]. In this case, the effective dark energy equation of state is indistinguishable from -1 and the expansion history is practically the same as in the lambda cold dark matter (ΛCDM) model. Furthermore, as long as the scalar field is at its density-dependent minimum, $\phi(\rho)$, the theory can be described parametrically from the sole knowledge of the mass function $m(\rho)$ and the coupling $\beta(\rho)$ at the minimum of the potential [17,18]

$$\frac{\phi(\rho) - \phi_c}{m_{\rm Pl}} = \frac{1}{m_{\rm Pl}^2}\int_{\rho}^{\rho_c} d\rho \frac{\beta(\rho)}{m^2(\rho)}, \tag{5}$$

where we have identified the mass as the second derivative

$$m^2(\rho) = \left.\frac{d^2 V_{\rm eff}}{d\phi^2}\right|_{\phi=\phi(\rho)} \tag{6}$$

and the coupling

$$\beta(\rho) = m_{\rm Pl}\left.\frac{d\ln A}{d\phi}\right|_{\phi=\phi(\rho)}. \tag{7}$$

It is often simpler to characterize the functions $m(\rho)$ and $\beta(\rho)$ using the time evolution of the matter density of the Universe

$$\rho(a) = \frac{\rho_0}{a^3} \tag{8}$$

where a is the scale factor whose value now is $a_0 = 1$. This allows one to describe characteristic models in a simple way and the full dynamics can be recovered from the time evolution of the mass and coupling functions, $m(a)$, $\beta(a)$.

A. Evolution of linear perturbations

While the scalar-tensor theories considered in this work predict the same expansion history as ΛCDM, the existence of the additional scalar interaction gives them distinguishing features in the evolution of linear matter and metric perturbations. More specifically, the attractive force mediated by the scalar enhances the overall growth of inhomogeneities. In addition, the relation between the curvature perturbation Φ and the Newtonian potential Ψ is modified [52]. Both of these effects can be captured in terms of two phenomenological functions employed in MGCAMB[1] [25,34,54], parametrizing effective modifications to the Poisson and the anisotropy Einstein equations in Fourier space. Namely, one defines $\mu(a,k)$ and $\gamma(a,k)$, such that

$$k^2\Psi = -4\pi G a^2 \mu(k,a)\rho\Delta, \tag{9}$$

$$\frac{\Phi}{\Psi} = \gamma(k,a) \tag{10}$$

where Δ is the comoving matter density contrast.[2] In the quasistatic approximation, whose validity is discussed below, functions $\mu(k,a)$ and $\gamma(k,a)$ can be expressed in terms of $m(a)$ and $\beta(a)$ as [18]

$$\mu(a,k) = A^2(\phi)(1 + \epsilon(k,a)), \tag{11}$$

$$\gamma(a,k) = \frac{1 - \epsilon(k,a)}{1 + \epsilon(k,a)}, \tag{12}$$

where

$$\epsilon(k,a) = \frac{2\beta^2(a)}{1 + m^2(a)a^2/k^2}. \tag{13}$$

The conformal factor $A^2(\phi)$ that appears in Eq. (11) is indistinguishable from unity for viable models within the class of scalar-tensor theories considered in this paper, and can be safely ignored. ΛCDM is recovered when $\epsilon \to 0$ and $\mu = \gamma = 1$.

In the quasistatic approximation, the equation governing the evolution of matter density contrast δ reads

$$\delta'' + \mathcal{H}\delta' - \frac{3}{2}\Omega_m \mathcal{H}^2 \mu(k,a)\delta = 0 \tag{14}$$

where $'$ is the derivative with respect to conformal time and $\mathcal{H} = a'/a$. Two regimes can be distinguished. When the mode k is outside the Compton wavelength of the scalar field, i.e. $k \ll am(a)$, $\epsilon \ll 1$ and the growth is not modified. Inside the Compton wavelength, $k \gg am(a)$, gravity is enhanced by $1 + 2\beta^2(a)$, implying more growth. In addition, in the symmetron and dilaton models, the

[1] MGCAMB is a publicly available patch to CAMB [53].

[2] These equations are valid at late times, when the contribution of relativistic species can be neglected. Equations used in MGCAMB are more general and are valid at all times [35].

coupling $\beta(a)$ depends on the matter density and controls the transition to the enhanced growth.

Since ϵ is a manifestly non-negative number, the growth is generically enhanced. Also, generically, $\gamma < 1$ in these models. At the same time, the relation between the lensing potential $\Phi + \Psi$ and the matter density is effectively unchanged. Namely, if one defines $\Sigma(k, a)$ as

$$k^2(\Psi + \Psi) = -8\pi G a^2 \Sigma(k, a)\rho\Delta, \tag{15}$$

then

$$\Sigma = A^2(\phi) \tag{16}$$

and is effectively unity for all viable modes. Thus, a clear detection of $\Sigma \neq 1$ would not only signal a breakdown of ΛCDM but would rule out the entire class of GBD models. We note that, even though Σ is constrained to be very close to unity in viable GBD models, its time derivative, $\dot{\Sigma}$, can, in principle, be non-negligible and affect the observables via the integrated Sachs-Wolfe (ISW) effect.

When functions $m(a)$ and $\beta(a)$ are regular, which is the case for chameleon models such as $f(R)$, and for dilatons, the error introduced by working in the quasistatic approximation scales as H/k [55]. For models such as the symmetron, in which the functions $m(a)$ and $\beta(a)$ vanish with a power $n < 1$ for $a > a_\star$ and are zero for $a < a_\star$ (and thus have a diverging derivative at $a_\star$), the accuracy is reduced to $(H/k)^n$ [55,56].

We note that an alternative way of parametrizing general modifications of gravity on linear scales is offered by the "effective field theory" approach of [57,58] implemented in the publicly available code EFTCAMB [59,60]. EFTCAMB parametrizes additional terms in the action, while MGCAMB is based on parametrizing modifications of the equations of motion. The latter is more directly related to observables and is better suited for the $[m(a), \beta(a)]$ parametrization adopted in this paper.

B. Functions $m(a)$ and $\beta(a)$ in $f(R)$

In what follows, we briefly motivate specific functional forms of $m(a)$ and $\beta(a)$ adopted for the analysis in Secs. III and IV. Given the forms of $m(a)$ and $\beta(a)$, the predictions for the observables can be calculated using MGCAMB [54]. Plots of the CMB temperature anisotropy and the matter power spectra for a few representative models are shown in Fig. 1.

Among theories exhibiting chameleon screening are the $f(R)$ class of models [61,62] described by the action

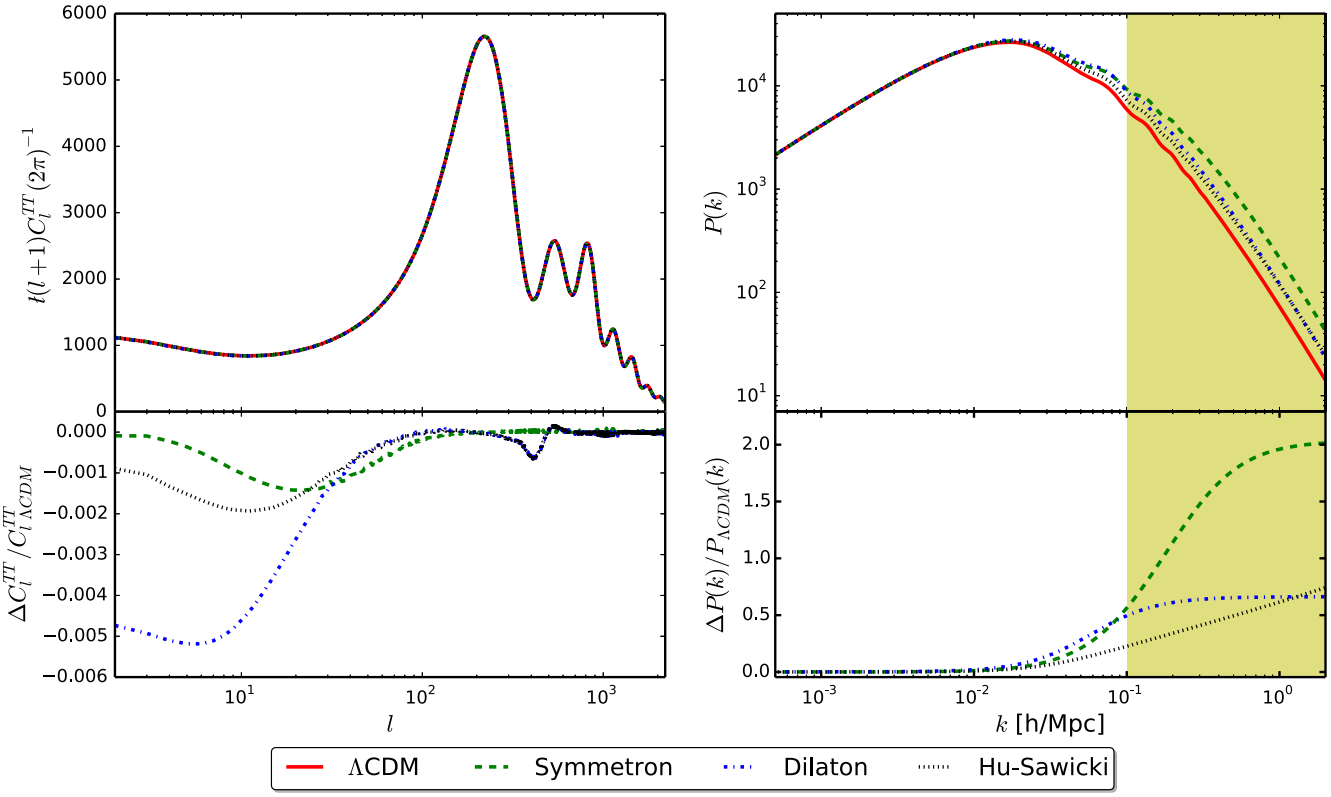

FIG. 1. Plots of CMB temperature anisotropy C_l^{TT} (left) and the matter power spectrum $P(k)$ (right) for the models studied in this paper. The parameters used for the symmetron model are $a_\star = 0.25, \beta_\star = 1$ and $\xi_\star = 10^{-3}$. The parameters used for the dilaton model are $\beta_0 = 3$ and $\xi_0 = 6 \times 10^{-3}$. The parameters used for the Hu-Sawicki $f(R)$ model are $f_{R_0} = 10^{-4}$ and $n = 1$. The yellow shaded region shows the scales that are not taken into account in the data analysis.

$$S = \int d^4x\sqrt{-g}\left[\frac{f(R)}{16\pi G} + L_m[\psi, g_{\mu\nu}]\right] \tag{17}$$

where the function $f(R)$ is designed to depart from the Einstein-Hibert form at smaller values of the curvature R. As a specific example, we take the form proposed by Hu and Sawicki (HS) [12],

$$f(R) = R - 2\Lambda + \frac{f_{R_0}}{n}\frac{R_0^{n+1}}{R^n}, \tag{18}$$

where Λ is the cosmological constant term, R_0 is the value of the curvature today and $f_{R_0} \equiv (1 - df/dR)_{R=R_0}$. As argued in [12,63,64], all viable $f(R)$ models should be of such "disappearing cosmological constant" type [64], and models similar to HS were proposed in [63,64].

For all $f(R)$ models, $\beta(a) = 1/\sqrt{6}$, while the mass function is model dependent. In the HS model, we have

$$m(a) = m_0\left(\frac{4\Omega_\Lambda + \Omega_m a^{-3}}{4\Omega_\Lambda + \Omega_m}\right)^{(n+2)/2} \tag{19}$$

where Ω_Λ and Ω_m are the dark energy and matter density fractions today, and m_0 is a mass scale that can be expressed in terms of f_{R_0} as [18]

$$m_0 = H_0\sqrt{\frac{4\Omega_\Lambda + \Omega_m}{(n+1)f_{R_0}}}. \tag{20}$$

Local tests of gravity require $f_{R_0} \lesssim 10^{-6}$ [49], while astrophysical constraints from dwarf galaxies imply that $f_{R_0} \lesssim 10^{-7}$ [47]. These bounds depend on accurate modeling of nonlinear physics. In what follows, we will derive the constraint on f_{R_0} from current cosmological data using only information from linear scales, and also forecast constraints expected from future surveys like LSST.

Representative CMB and matter power spectra for $f(R)$ are shown in Fig. 1. A notable effect on the CMB spectrum is the suppression of power at small multipoles, which is due to the reduced ISW effect. The magnitude of the ISW effect is proportional to the net change in the gravitational potential along the line of sight. In ΛCDM, the change in the potential is a reduction caused by the onset of cosmic acceleration. In $f(R)$, the additional scalar force enhances the potential which, combined with the decay due to acceleration, leads to a smaller net change and, thus, a smaller ISW effect. The other notable impact of $f(R)$ on the CMB spectrum is the enhanced lensing, which has the effect of slightly dumping the peaks. The enhanced growth is more evident in the plot of $P(k)$. Qualitatively, these features are common to all GBD models.

C. Functions $m(a)$ and $\beta(a)$ for the dilaton

Another relevant example is the environmentally dependent dilaton [14], where the screening mechanism is of the Damour-Polyakov type [16]. This model, inspired by string theory in the large string coupling limit, has an exponentially runaway potential

$$V(\phi) = V_0 e^{-\phi/m_{\rm Pl}}, \tag{21}$$

with the value of V_0 set to generate the current acceleration of the Universe, while the coupling function is

$$A(\phi) = 1 + \frac{A_2}{2m_{\rm Pl}^2}(\phi - \phi_\star)^2. \tag{22}$$

In dense environments, the minimum of the effective potential approaches $\phi = \phi_\star$, and the coupling function $\beta(a)$ vanishes. The coefficient A_2 has to be large to satisfy local tests of gravity; typically $A_2 \gtrsim 10^6$. These models can be described by a mass function given by

$$m^2(a) = 3A_2H^2(a) \tag{23}$$

and, assuming matter domination, a coupling function

$$\beta(a) = \beta_0 a^3, \tag{24}$$

where $\beta_0 = \Omega_\Lambda/\Omega_m \sim 2.7$ is related to V_0, and is determined by requiring that ϕ play the role of dark energy. We will present our constraints on the mass in terms of a scalar-force range parameter ξ_0, defined as

$$\xi_0 = \frac{H_0}{cm_0} = \frac{1}{\sqrt{3A_2}}, \tag{25}$$

where $m_0 = m(a = 1)$. We show representative CMB and matter power spectra for the dilaton model in Fig. 1, with parameter values being large on purpose to exaggerate the qualitative features of the model.

D. Functions $m(a)$ and $\beta(a)$ for symmetrons

Another example of a GBD model with the Damour-Polyakov screening mechanisms is the symmetron [15], where the scalar field has a quartic potential,

$$V(\phi) = V_0 + \frac{m_\star^2\phi_\star^2}{2}\left[-\frac{1}{2}\left(\frac{\phi}{2\phi_\star}\right)^2 + \frac{1}{4}\left(\frac{\phi}{\phi_\star}\right)^4\right] \tag{26}$$

and a coupling function,

$$A(\phi) = 1 + \frac{\beta_\star}{2\phi_\star}\phi^2. \tag{27}$$

When matter density is large, the effective potential has a minimum at $\phi = 0$ and $A(\phi) \to 1$, thus decoupling the

scalar from matter. At lower densities, the effective potential acquires a nonzero minimum, activating the scalar force. For cosmological densities, the transition occurs at

$$\rho_\star = \frac{\rho_m}{a_\star^3} = \frac{m_{pl} m_\star^2 \phi_\star^2}{2\beta_\star}, \tag{28}$$

where ρ_m is the matter density today. Thus, one can work with $a_\star$, along with $m_\star$ and $\beta_\star$, as the three free parameters of the theory. At $a > a_\star$, the model can be described by

$$m(a) = m_\star \sqrt{1 - \left(\frac{a_\star}{a}\right)^3} \tag{29}$$

and

$$\beta(a) = \beta_\star \sqrt{1 - \left(\frac{a_\star}{a}\right)^3}, \tag{30}$$

while $\beta(a) = 0$ for $a < a_\star$. As in the case of dilatons, we represent our bounds in terms of a range parameter $\xi_\star$, defined as

$$\xi_\star = \frac{H_0}{c}\frac{1}{m_\star}. \tag{31}$$

Representative CMB and matter power spectra for this model are shown in Fig. 1.

E. Generalized chameleon models

In our forecasts, we will also consider generalized models of chameleon type [65] defined by

$$m(a) = m_0 a^{-r}, \qquad \beta(a) = \beta_0 a^{-s}. \tag{32}$$

In practically all viable chameleon models, the coupling function is expected to vary extremely slowly at redshifts probed by large scale structure surveys. Thus, for all practical purposes, it can be taken to be a constant of order unity.

F. Binned model

As discussed so far, for any of the aforementioned models, each with its own theoretical motivation, one can determine the functional forms of $m(a)$ and $\beta(a)$. This effectively reduces the two free functions $m(a)$ and $\beta(a)$ to a handful of parameters. However, one might be interested in knowing how well the two functions are constrained in general, without regard for any specific model. One can then proceed by discretizing either of the two functions in bins of redshift space and treating the amplitude in each bin as a free parameter to be constrained.

Varying both the coupling and the mass functions simultaneously would be redundant, since their effect is largely degenerate. Since it is the mass parameter that affects the shape of the matter power spectrum, we fix $\beta(a)$ to a constant value of order unity and bin $m(a)$ in redshift. If a nonzero $m^{-1}(a)$ were detected, it would signal the presence of a scalar interaction and further investigation would be required to determine if the variation occurs in $\beta(a)$, $m(a)$ or both.

While a binning scheme gives a model-independent (rather a far less model-dependent) treatment of $m(a)$, the larger number of parameters (values of m in each bin) results in weaker constraints on the individual parameters. To extract useful information, we apply the principal components analysis (PCA) technique (reviewed in Sec. IV G). The resulting principal components (PCs) are linear combinations of the original bin values and the propagated uncertainty (from original errors on the bins) in their values can inform us about those PCs that are best constrained by data and the number of degrees of freedom that can potentially be constrained.

III. CONSTRAINTS FROM CURRENT DATA

In this section, we use a combination of currently available CMB, lensing and baryonic acoustic oscillation (BAO) data, as well as measurements of the matter power spectrum, to derive constraints on the GBD parameters. To compute the observables, we implemented the parametrizations described in the previous section in MGCAMB. We then use it with an appropriately modified version of CosmoMC [66] to obtain the posterior distributions for the model parameters. Since current data are unable to simultaneously constrain multiple GBD parameters, we will only consider models from the previous section for which meaningful constraints are possible.

A. The data sets used in the analysis

We use the measurements of CMB temperature anisotropy from the second release of the *Planck* survey [67] in the form of the *Planck* high-ℓ temperature power spectrum (TT) likelihood ($30 < \ell < 2500$) along with the low-ℓ polarization ($\ell < 30$). We refer to the above data sets as PLC. We also consider the *Planck* 2015 lensing potential spectrum [68] extracted from mode-coupling correlations, and refer to this data set as CMBLens.

In addition to inducing higher order correlations, lensing by large scale structures affects the TT spectrum at higher ℓ, slightly damping the oscillatory features. In [69], and subsequently in [67], the lensing contribution to TT was quantified via an amplitude A_L multiplying the lensing power spectrum in the calculation of the theoretical prediction for TT. The parameter A_L was used to quantify the significance of detection of the lensing contribution to TT. However, instead of measuring the expected value of $A_L = 1$, since the lensing contribution to TT is calculated from the same model as the rest of the spectrum, the best fit

value obtained for ΛCDM from the PLC data set in [67] was $A_L = 1.22 \pm 0.10$, or two standard deviations away from the expectation. As discussed in [69] (see also [70]) this is due to an apparent tension between the higher-ℓ and lower-ℓ data when trying to fit ΛCDM to Planck TT data. To negate the effect of this tension, the parameter A_L was sometimes covaried with other parameters when deriving constraints on ΛCDM in [67]. In what follows, we take the view that A_L is not a physical parameter and should be held fixed to 1 when deriving constraints on cosmological models. However, we also investigate and discuss the effect of covarying A_L in the case of $f(R)$.

For BAO measurements, we used data from the 6dF survey [71] and from SDSS, specifically the MGS [72] and BOSS data releases (LOWZ and CMASS) [73].

We also use the matter power spectrum (referred to as MPK) from SDSS LRG DR4 [74], but only on linear scales, $k \leq 0.1\ h/\mathrm{Mpc}$. We are aware of the fact that nonlinear corrections can play a role even at $k \lesssim 0.1$ Mpc and that a proper treatment of the bias and the redshift space distortions (RSD) must take them into account. This was studied at length in [75] for the SDSS DR9 power spectrum and it was found that the differences in the upper bounds on neutrino masses obtained using four different RSD models were under 20%. Based on this, we expect that bounds on the GBD parameters (such as f_{R_0}) obtained from MPK are accurate to within 30%, which is sufficient given that constraints from current data are relatively weak.

Finally, we consider the weak lensing data from the Canada France Hawaii Telescope Lensing Survey 2DCFHTLenS [76], referred to as WL. To avoid dealing with nonlinear scales, we adopt a conservative cut and exclude $\theta < 30'$ from the measurements of the correlation function $\xi^{\pm}$, which corresponds to $k < 0.1\ h/\mathrm{Mpc}$ scales.

B. Constraints on $f(R)$

The Hu-Sawicki $f(R)$ model has two parameters, f_{R_0} and n. In what follows, we fix $n = 1$ because that is a common choice in the literature, and also because the two parameters are highly correlated and the current data cannot simultaneously constrain both. We chose a flat prior on $\log_{10} f_{R_0}$ within the $[-7, 0]$ range. We have checked that changing the range of the flat prior does not affect our results.

Figure 2 shows constraints on f_{R_0} for different combinations of data sets described in Sec. III A, after marginalizing over all the other cosmological parameters. We considered the case in which the total neutrino mass is fixed at $\sum m_\nu = 0.06$ eV (solid lines), and the case where it can vary within $0 \leq \sum m_\nu \leq 1$ eV (dashed lines). The results from Fig. 2 are summarized in Table I.

We can see that the combination of PLC and BAO data sets (blue lines) only weakly constrains the model. Modified gravity affects the CMB temperature anisotropy spectrum in two ways: it affects the low-ℓ power spectrum through the ISW effect and enhances the damping at high-ℓ due to the enhancement in clustering and, as a consequence, the lensing potential. Thus, the observed lack of power at low-ℓ multipoles and the apparent preference of enhanced lensing in CMB TT, when compared to the ΛCDM prediction, can be reconciled by a nonzero f_{R_0}. This is the reason for the peak in the PLC + BAO likelihood. Adding the CMBLens data (red lines) tightens the constraint substantially. The enhancement of growth due to the extra scalar interaction affects the lensing potential measured by *Planck*, which is known to be in excellent agreement with the ΛCDM prediction [68]. Thus, the weak preference for larger f_{R_0} coming from PLC + BAO is overwhelmed by the stronger CMBLens data that are consistent with $f_{R_0} = 0$.

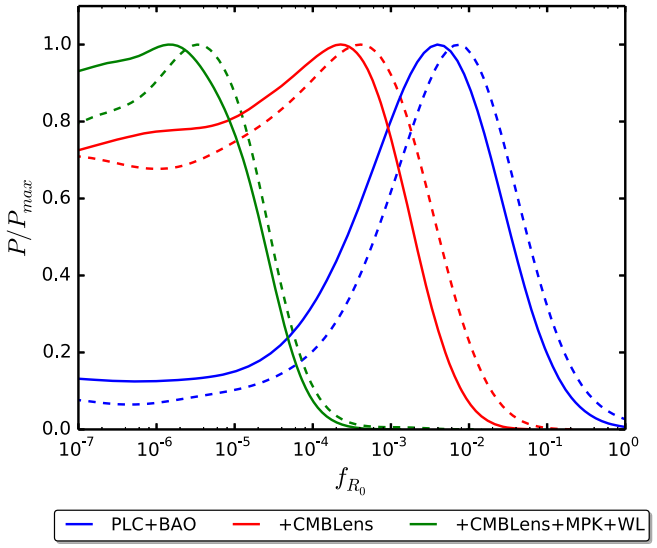

FIG. 2. The marginalized posterior distribution for the f_{R_0} parameter in the Hu-Sawicki model ($n = 1$) for different combinations of data sets. The solid lines show the PDF in the case of massive neutrinos with a fixed mass $\sum m_\nu = 0.06$ eV, while the dashed lines show the PDF for the case when the neutrino mass was varying. Due to the degeneracy between f_{R_0} and $\sum m_\nu$, we see that the constraint on f_{R_0} becomes weaker when the neutrino mass is varied. The data sets are labeled according to the notation introduced in Sec. III A. The symbol + means that we add data on top of the PLC + BAO data set. For example, +lensing means PLC + BAO + lensing.

TABLE I. The 68% (95%) C.L. upper limits of f_{R_0} and the sum of neutrino masses using different combinations of data sets shown in the table.

	Fixed $\sum m_\nu$	Varying $\sum m_\nu$	
Data sets	f_{R_0}	f_{R_0}	$\sum m_\nu$ (eV)
PLC + BAO	0.05(0.14)	0.08(0.23)	0.24(0.35)
+CMBLens	$3(8) \times 10^{-3}$	$0.6(1.6) \times 10^{-2}$	0.22(0.31)
+MPK	$0.6(1.6) \times 10^{-4}$	$0.7(1.7) \times 10^{-4}$	0.24(0.34)
+WL	$3(7) \times 10^{-5}$	$4(9) \times 10^{-5}$	0.23(0.33)

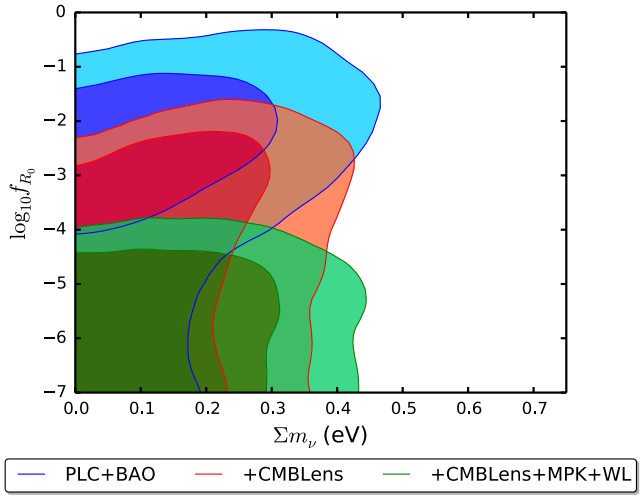

FIG. 3. Joint contours for f_{R_0} and $\sum m_\nu$ in the Hu-Sawicki model ($n = 1$) after marginalizing over all other cosmological parameters. The darker and lighter shades correspond respectively to the 68% C.L. and the 95% C.L. Data sets are described in text and also in the caption of Fig. 2.

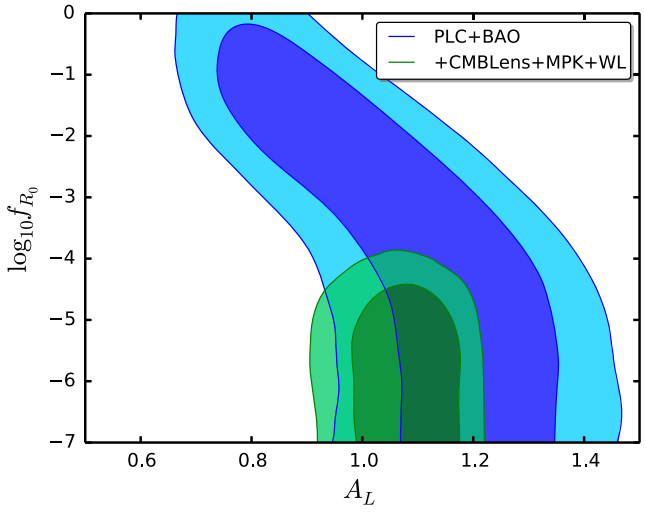

FIG. 4. Joint contours for f_{R_0} and A_L in the Hu-Sawicki model. The darker and lighter shades correspond respectively to the 68% C.L. and the 95% C.L. Using PLC + BAO data sets only it is possible to detect high values of f_{R_0} that can cure the tension in lensing amplitude A_L. However such high values are ruled out once we add lensing and LSS data sets.

The constraint becomes even tighter after adding the MPK and WL data sets (green lines).

The dashed lines in Fig. 2 show the impact of covarying the combined mass of neutrinos, $\sum m_\nu$, along with f_{R_0}. Massive neutrinos suppress the growth and can partially compensate for the enhanced clustering in $f(R)$, slightly weakening the bounds on f_{R_0}. The extent of the degeneracy can be inferred from Fig. 3 which shows the joint confidence contours for the two parameters. We see that, although the constraint on f_{R_0} becomes tighter as we add the LSS data, the constraint on $\sum m_\nu$ remains roughly the same. This is because we are restricting our analysis to linear scales, while the effect of massive neutrinos becomes more relevant on smaller scales and, hence, causes only a small degradation of f_{R_0} constraints.

Up to this point, we kept the unphysical lensing amplitude parameter A_L fixed at its expected value of 1. However, one may wonder if the discrepancy in A_L observed in the ΛCDM model also persists in $f(R)$, and what effect covarying A_L has on the bounds on f_{R_0}. The results for two different combinations of data are shown in Fig. 4. Although it seems that, in the case of PLC + BAO, the lensing amplitude tension has been reconciled, we argue that this is not due to a genuine signal of modified gravity. As discussed previously, the PLC + BAO data yield a peak in the likelihood of f_{R_0} because the preference for enhanced lensing and the lack of power at low ℓ in C_ℓ^{TT} can be reconciled with a nonzero f_{R_0}. The enhanced lensing appears to cure the A_L problem and this is depicted in Fig. 4, where we see that there is a strong degeneracy between A_L and f_{R_0} for large values of the latter (blue contours). However such large values of f_{R_0} are ruled out once we add the data sets that probe clustering (green contours). Still, the value of A_L when cofit with f_{R_0} is in better disagreement with the prediction. For the combination of all data we find

$$A_L = 1.11^{+0.20}_{-0.14} \qquad 68\%\,\text{C.L.}, \quad \text{all data sets.} \qquad (33)$$

The results of the analysis with varying A_L are summarized in Table II.

C. Constraints on the symmetron model

In this subsection we derive constraints on the inverse mass parameter, $\xi_\star$, defined in Eq. (31), which represents the Compton wavelength of the scalar interaction. We fix the other two symmetron parameters, taking $a_\star = 0.25$ and $\beta_\star = 1$, since current data are unable to constrain them simultaneously with $\xi_\star$.

Figure 5 shows the posterior probability distribution for the $\xi_\star$ parameter with a fixed $\sum m_\nu = 0.06$ eV (red solid line) as well as after marginalizing over a varying $\sum m_\nu$ (blue dashed line). We find an upper bound of $\xi_\star < 1.5 \times 10^{-3}$ at 95% C.L., which corresponds to a Compton

TABLE II. 68% (95%) C.L. bounds on f_{R_0}, A_L and $\sum m_\nu$ using all the data sets: PLC + BAO + CMBlens + MPK + WL.

$f(R)+A_L$, fixed $\sum m_\nu$		$f(R)+A_L$, varying $\sum m_\nu$		
f_{R_0}	A_L	f_{R_0}	A_L	$\sum m_\nu$
$3(8)\times10^{-5}$	$1.08^{+0.07(0.12)}_{-0.05(0.13)}$	$0.4(1.0)\times10^{-4}$	$1.11^{+0.10(0.16)}_{-0.06(0.15)}$	0.30(0.38)

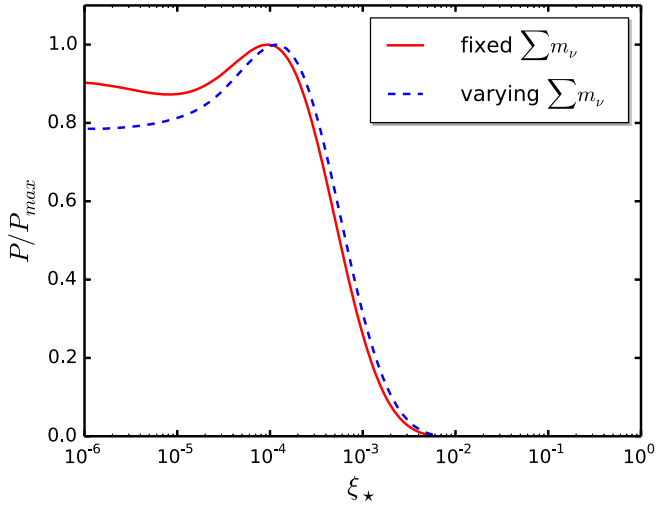

FIG. 5. The marginalized posterior distribution for $\xi_\star$ in symmetron model with $\beta_\star = 1$ and $a_\star = 0.25$ considering neutrinos with $\sum m_\nu = 0.06$ eV (red solid line) and marginalizing over a varying $\sum m_\nu$ (blue dashed line). The data sets used in this analysis are PLC + BAO + lensing + MPK + WL as described in Sec. III A.

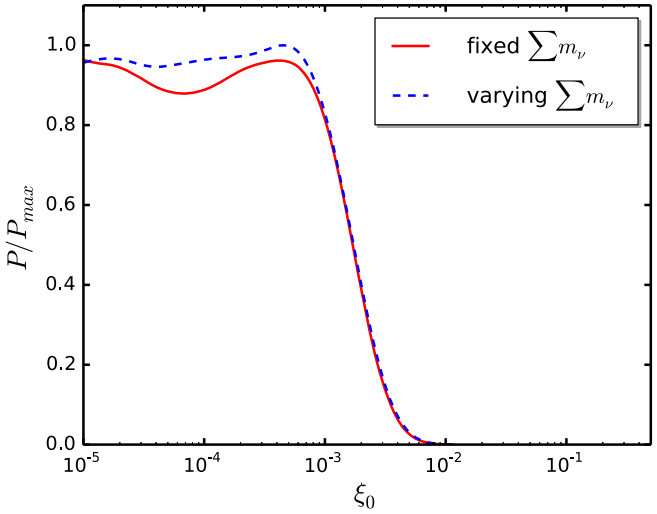

FIG. 6. Marginalized posterior distribution for ξ_0 in the dilaton model with $\beta_0 = 5$. The data sets used in the analysis are PLC + BAO + lensing + MPK + WL as described in Sec. III A. The red solid line shows the case with massive neutrinos with a fixed mass of $\sum m_\nu = 0.06$ eV, while the blue solid lines show the PDF after marginalizing over a varying $\sum m_\nu$.

wavelength of ∼ a few Mpc. Our bounds are summarized in Table III.

As mentioned above, current data are unable to simultaneously constrain all the model parameters because they are highly correlated. We also note that one cannot derive meaningful constraints for smaller values of coupling constant $\beta_\star$ as the modification of growth is relatively small for the scales and redshifts currently probed. Further, since $a_\star$ sets the onset of modified growth, we would see tighter constraints on $\xi_\star$ for smaller $a_\star$ values. Nevertheless, as we will show in Sec. IV, future surveys with larger sky and deeper redshift coverage will be able to constrain $\xi_\star$ along with the other two parameters.

D. Constraints on the dilaton model

Analogously to the symmetron model, we constrain the inverse mass parameter ξ_0 defined by Eq. (25), and fix β_0 to a constant. Figure 6 shows the posterior distribution for ξ_0 with the current value of the coupling parameter fixed at $\beta_0 = 5$. We find an upper bound of $\xi_0 < 3 \times 10^{-3}$ (95% C.L.). As for symmetrons, the sensitivity to the coupling is weak due to the lack of data on linear scales. However, as we will see in Sec. IV, constraints will improve significantly with future surveys. Our results for the dilaton model are summarized in Table III.

TABLE III. Summary of the 95% C.L. upper limits of the MG parameters and the sum of neutrino masses (in units of eV) derived from current observations described in Sec. III A.

	Fixed $\sum m_\nu$	Varying $\sum m_\nu$	
Symmetron	$\xi_\star$ $0.8(1.5) \times 10^{-3}$	$\xi_\star$ $0.9(1.8) \times 10^{-3}$	$\sum m_\nu$ 0.16(0.27)
Dilaton	ξ_0 $2.1(3) \times 10^{-3}$	ξ_0 $2.3(3) \times 10^{-3}$	$\sum m_\nu$ 0.15(0.25)

IV. FORECASTS

Constraints on scalar gravitational interactions derived in the previous section, using current information available on linear scales, are relatively weak when compared to bounds available from astrophysical tests. With improved redshift resolution, depth and sky coverage that future surveys will provide, the number of modes in the linear regime will dramatically increase. Thus, it is interesting to know if future constraints from linear scales can become compatible with astrophysical bounds.

In what follows, we perform a series of Fisher forecasts for the model parameters described in the previous section, using, where possible, the current bounds on model parameters as fiducial values in the forecast. Where there was no upper bound, we use fiducial values motivated by a combination of theoretical considerations and existing constraints from nonlinear scales. We also perform a principal component analysis (PCA) of $m(a)$ for a fixed order unity coupling β, to see how well future data sets can constrain an evolving mass parameter.

A. The data assumed in the forecast

The data we consider in our forecast include CMB temperature anisotropy (T) and polarization (E) power spectra with characteristics of the Planck survey, weak lensing shear (WL) and galaxy number count (GC) from a

LSST-like survey [50], with the survey parameters adopted from [77], and their cross-correlations. In some cases, we compare this to constraints expected from the Dark Energy Survey (DES) [78].

Theoretical power spectra are calculated assuming the LSST (DES) GC data are partitioned into 10 (4) tomographic redshift bins, while the WL shear field is split into 6 (4) tomographic redshift bins. In addition, we assume a flat Friedmann-Robertson-Walker geometry and vary h, $\Omega_c h^2$, $\Omega_b h^2$, τ, n_s, w and A_s, together with the modified gravity parameters. The fiducial values of the cosmological parameters are taken to be the Planck 2015 best fit results. To calculate the WL and GC auto- and cross-correlation spectra in our scalar-tensor models, we have applied the MGCAMB patch to CAMBSources [79]. The details of the implementation are described in [25,35].

B. Fisher analysis

For a given model, one can calculate the Fisher matrix [80] to determine how well future surveys can constrain its parameters. The inverse of the Fisher matrix provides a lower bound on the covariance matrix of the model parameters via the Cramér-Rao inequality, $\mathbf{C} \geq \mathbf{F}^{-1}$. For zero-mean Gaussian-distributed observables, such as the angular correlations C_ℓ^{XY}, the Fisher matrix is given by

$$F_{ab} = f_{\rm sky} \sum_{\ell=\ell_{\rm min}}^{\ell_{\rm max}} \frac{2\ell+1}{2} \mathrm{Tr}\left(\frac{\partial C_\ell}{\partial p_a} \tilde{C}_\ell^{-1} \frac{\partial C_\ell}{\partial p_b} \tilde{C}_\ell^{-1}\right), \quad (34)$$

where p_a is the ath parameter of our model and $\tilde{\mathbf{C}}_\ell$ is the "observed" covariance matrix with elements $\tilde{C}_\ell^{XY}$ that include contributions from noise:

$$\tilde{C}_\ell^{XY} = C_\ell^{XY} + N_\ell^{XY}. \quad (35)$$

Equation (34) assumes that all fields $X(\hat{\mathbf{n}})$ are measured over contiguous regions covering a fraction $f_{\rm sky}$ of the sky. The value of the lowest multipole can be approximately inferred from $\ell_{\rm min} \approx \pi/(2f_{\rm sky})$. The noise matrix N_ℓ^{XY} includes the statistical noise as well as the expected systematic errors. We refer the reader to [25,35] for the details of the Fisher matrix calculations for the individual experiments considered in our analysis.

C. The *f(R)* forecast

In Fig. 7 we show 1σ constraints on parameters of the Hu-Sawicki $f(R)$ model, as expected from LSST + (LSST WL + LSST GC + Planck CMB). Recall that current data are unable to constrain f_{R_0} unless one assumes a fixed value for n, since the two parameters are highly degenerate. Thus, the forecast in Fig. 7 depends strongly on the assumed fiducial value, indicated with a $\star$ on the plot. What we see is that for $n \sim 1$ or smaller, future data will be able to constrain both parameters simultaneously.

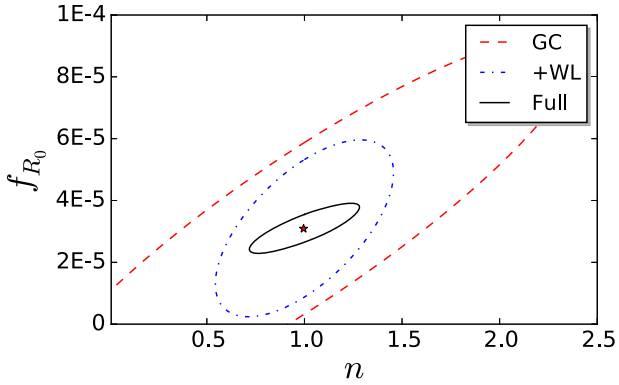

FIG. 7. Expected 1σ bounds on the parameters of the Hu-Sawicki model. The assumed fiducial model is marked with a star. The importance of using the "full" set of observables (WL, GC and their cross-correlation) is clearly demonstrated. The Planck CMB data are included in all cases and are important for constraining the standard cosmological parameters.

Figure 7 also shows the importance of including the cross-correlation between WL and GC. The information from GC alone is largely diluted by the unknown galaxy bias. Weak lensing, while not sensitive to the bias, is plagued by degeneracies coming from projection effects. Combining them helps determine the bias and break the degeneracies coming from projections.

Figure 8 compares joint 1σ constraints on f_{R_0} and the combined mass of neutrinos, $\sum m_\nu$, as expected from LSST+ vs those expected from DES+. We see that LSST+ can reduce uncertainties in both parameters by a factor of 3. The plot shows the effect of marginalizing over n; however the outcome depends on the assumed fiducial value of n (which is $n = 1$).

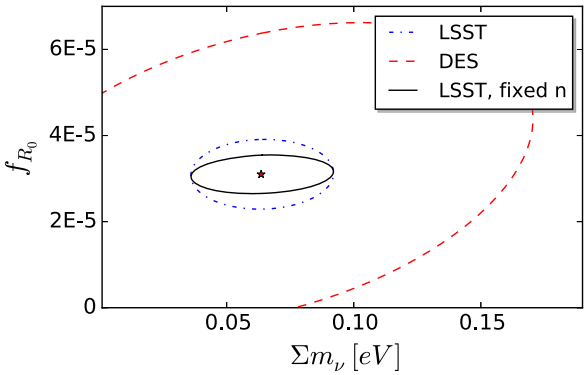

FIG. 8. Comparison of the uncertainties expected from LSST+ vs those from DES+ for the f_{R_0} parameter of the $n = 1$ Hu-Sawicki model and the total mass of neutrinos. The assumed fiducial model is marked with a star. The effect of fixing n, as opposed to marginalizing over it, is also shown.

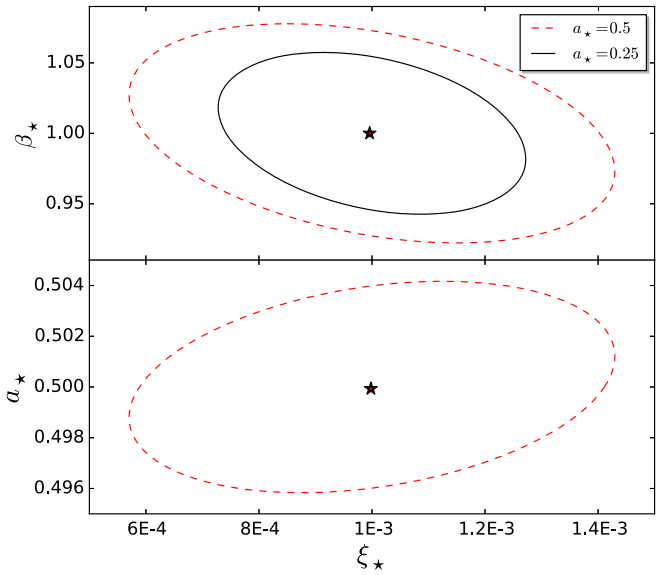

FIG. 9. Expected 1σ constraints from LSST+ on the parameters of the symmetron model. The assumed fiducial models are marked with a star. Unlike current data, LSST+ can simultaneously constrain $\beta_\star$ and $a_\star$ to a few percent level, and will improve the current bounds on $\xi_\star$. See Table IV for a quantitative comparison.

D. The symmetron forecast

Figure 9 shows the bounds on the parameters of the symmetron parameters expected from LSST+. As a fiducial model, we assume $\beta_\star = 1$ and a mass scale of $\xi_\star = 10^{-3}$, which corresponds to a range of a few Mpc. Current data are unable to constrain $\xi_\star$ if $a_\star = 0.5$ or larger. For this reason, the bound on $\xi_\star$ in Sec. III was derived for a fixed $a_\star = 0.25$. We perform a forecast using two different fiducial values: $a_\star = 0.25$ and 0.5. In the former case, LSST+ clearly improves on the bound in Sec. III, even after marginalizing over $a_\star$ and $\beta_\star$. It will also be able to provide a nontrivial bound on $\xi_\star$ for $a_\star = 0.5$, which is the value assumed in much of the previous literature. The current and expected bounds are summarized in Table IV.

It is interesting to examine the possible degeneracy between the symmetron parameters and the total mass of neutrinos. Figure 10 shows the joint uncertainties in $\xi_\star$ and $\sum m_\nu$ expected from LSST+ assuming a fiducial model with $\beta_\star = 1$, $\xi_\star = 10^{-3}$, $a_\star = 0.5$ and $\sum m_\nu = 0.06$ eV. It is clear from the figure that there is practically no degeneracy between $\xi_\star$ and m_ν which is because they affect the growth on different scales. Fixing the other MG parameters in this model, as opposed to marginalizing over them, does not change the degree of degeneracy; neither does it improve the constraints.

E. The dilaton forecast

Figure 11 shows expected bounds on the dilaton model parameters, with $\beta_0 = 1$ and $\xi_0 = 10^{-3}$ as the fiducial values. Similar to the symmetron case, we find that a LSST-like survey can constrain the inverse mass parameter ξ_0 to a percent level accuracy which is a significant improvement over current constraints. Constraints on the coupling constant β_0, however, are not as tight as those on $\beta_\star$ in the symmetron case. This is due to a lesser impact of the dilaton on the linear matter power spectrum. One can see from Fig. 1 that for the chosen fiducial values, $P(k)$ would deviate from the ΛCDM prediction far less in the dilaton case compared to the symmetron. The bottom panel in Fig. 11 shows the expected joint constraints on the neutrino masses, which are tighter than those for the symmetron. Again, this is because dilatons have a much lesser impact on the growth on linear scales.

F. The generalized chameleon model

Forecasts for the generalized chameleon provide a general estimate of how well one could constrain the scalar gravitational interactions with a next generation WL survey such as LSST. In Fig. 12 we show forecasted uncertainties on the parameters of the generalized chameleon model for two fiducial values of r, assuming that the coupling is constant ($s = 0$). For a slower evolution with time ($r = 1$), the scalaron mass decreases slower and modification to growth extends back to larger redshifts, leading to significantly tighter constraints. Thus, while LSST+ can constrain the coupling, the mass and the time variation of the scalaron mass simultaneously, the strength of the bounds depends strongly on the assumed fiducial model.

G. Principal component analysis of $m(a)$

In addition to considering particular functional forms of $\beta(a)$ and $m(a)$ as motivated by the scalar-tensor models mentioned in the preceding sections, it is also interesting to treat the coupling and the mass as two general functions and ask what features of these two functions can be

TABLE IV. The current 68% C.L. uncertainties and those expected from LSST+. The blocks with "–" mean the parameter was fixed at its fiducial value. The values in parentheses indicate those obtained for an alternative fiducial value.

	Hu-Sawicki $f(R)$		Symmetron			Dilaton	
Parameters	f_{R_0}	$n = 1$	$\xi_\star$	$\beta_\star = 1$	$a_\star = 0.25(0.5)$	ξ_0	$\beta_0 = 1(5)$
Current 1σ	4×10^{-5}	not applicable	10^{-3}	not applicable	not applicable	unconstrained (2.3×10^{-3})	not applicable
LSST + 1σ	6×10^{-6}	0.3	$2(2.9) \times 10^{-4}$	0.05 (0.07)	0.001 (0.005)	2.7×10^{-5}	2.3×10^{-1}

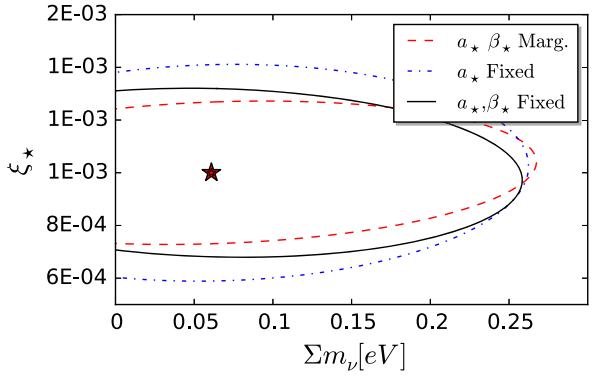

FIG. 10. Expected 1σ bounds on the $\xi_\star$ parameter of the symmetron model and the mass of neutrinos, $\sum m_\nu$. The assumed fiducial model is marked with a star. Fixing the other MG parameters in this model, as opposed to marginalizing over them, does not change the degree of degeneracy; neither does it improve the constraints.

constrained by the future data. In principle, one could discretize the functions $\beta(a)$ and $m(a)$ into N bins in a and treat the bins' values as free parameters. However, we find that even future data will not be able to simultaneously constrain $m(a)$ and $\beta(a)$ in a completely model-independent way, since the two parameters are largely degenerate in their effect on the observables on linear scales, as they appear together in $\epsilon(a,k)$ [see Eq. (13)]. For this reason, we fix β at a constant value of order unity and discretize $m(a)$ into bins with $m(a_i), i = 1,\ldots,N$.

As with earlier forecasts, we can calculate the Fisher matrix, and invert it to find the covariance matrix,

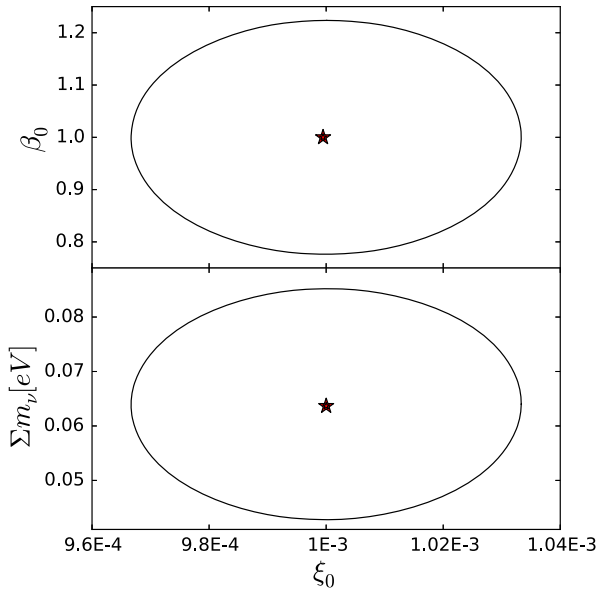

FIG. 11. 1σ bounds on the neutrino masses and parameters of the dilaton model expected from LSST+. The fiducial values are marked with stars.

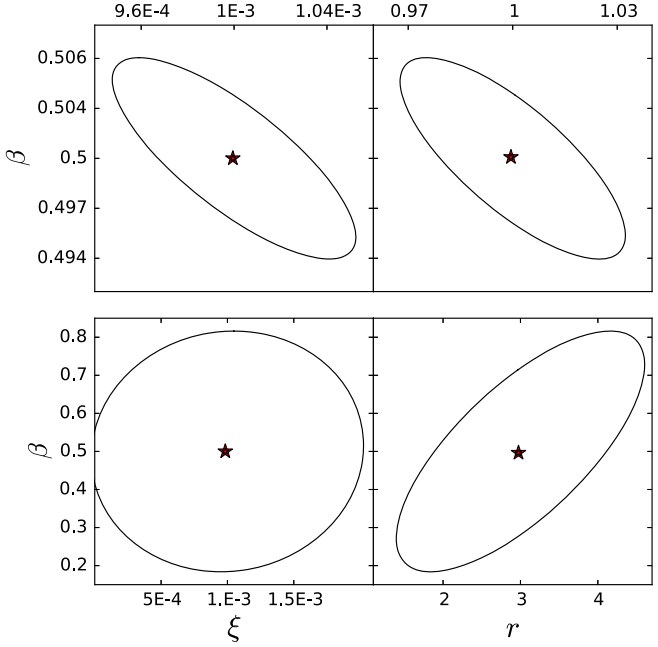

FIG. 12. Expected 1σ constrains on the generalized chameleon parameters for a fiducial model with $r = 3$ (top) and $r = 1$ (bottom) as a fiducial model. In each case, the value of r is varied and marginalized over.

$$C_{ij} \equiv \langle (p_i - \bar{p}_i)(p_j - \bar{p}_j) \rangle, \tag{36}$$

where $\bar{p}_i$ are the "fiducial" values, and parameters include the bins $m(a_i)$, as well as the rest of cosmological parameters. We then isolate the $N \times N$ block of the matrix, C^m, corresponding to the covariance of $m(a_i)$ after marginalization over other parameters. Since the individual bins of $m(a_i)$ bins are highly correlated, the covariance matrix for these parameters will be nondiagonal, and the value of m in any particular bin will be practically unconstrained. The principal component analysis (PCA) [27,35,36,81,82] is a way to decorrelate the parameters and find their linear combinations that are best constrained by data. Namely, we solve an eigenvalue problem to find a matrix W^m that diagonalizes C^m:

$$C^m = (W^m)^T \Lambda W^m; \qquad \Lambda_{ij} = \lambda_i \delta_{ij}, \tag{37}$$

where $W^m_{ij} \equiv \hat{e}_i(a_j)$ are the eigenvectors (or eigenmodes) and λ_i's are the eigenvalues. In the limit of large N, one can write an arbitrary $m(a)$ as an expansion into $\hat{e}_i(a)$:

$$m(a) - \bar{m}(a) = \sum_{i=1}^{N} \alpha_i \hat{e}_i(a) \tag{38}$$

in which case λ_i can be interpreted as the variance of α_i,

$$\lambda_i = \sigma^2_{\alpha_i}. \tag{39}$$

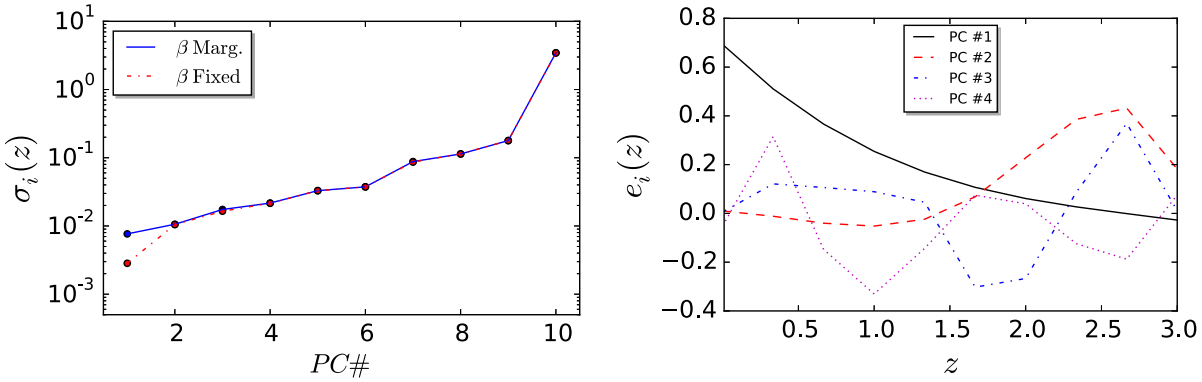

FIG. 13. Left: The uncertainties (square roots of eigenvalues) associated with the eigenmodes of $m(a)$ for the case when the coupling is fixed at $\beta = 0.4$ (solid line), and when it is marginalized over (dashed line). Right: The first four best constrained eigenmodes of $m(a)$ after marginalizing over β.

It is customary to order the eigenmodes from the best constrained to the worst. Then the ith eigenmode is referred to as the ith principal component (PC). Typically, one finds that only the first few modes are well constrained by the data, while most of them are practically unconstrained.

For our forecast, we partition $m(a)$ into 11 bins, with 10 of them evenly spaced in redshift within $z \in [0, 3]$, and the 11th bin ranging from $z = 3$ to $z = 30$. The last bin can be taken to be wide because the observables we work with are weakly sensitive to modifications at high redshifts. In what follows, we marginalize over the 11th bin, since it is largely degenerate with some of the cosmological parameters, most prominently with Ω_m. We take the fiducial model to be $\beta = 0.4$ and $m(a_i) = m_0$ for all i, with $m_0 = H_0/\xi c$ and $\xi = 10^{-3}$, corresponding to $m_0 = 0.2\ h/\mathrm{Mpc}$.

The left panel in Fig. 13 shows the forecasted uncertainties in the measurement of the eigenvectors for two cases: when β is fixed, and when β is marginalized over. In both cases, we marginalize over all cosmological parameters and the 11th m-bin. The right panel in Fig. 13 presents the first four best constrained eigenvectors of $m(a)$ after marginalizing over β. One can interpret the best constrained mode (PC1) as that corresponding to a weighted average value of $m(a)$. The second best constrained mode (PC2) has a single node and corresponds to the difference between the high-z and low-z values of $m(a)$. The third best mode (PC3) has 3 nodes, PC4 has 4 nodes, and so on.

The eigenvalue plot demonstrates that marginalizing over β affects the first eigenmode of $m(a)$, but not the others. This is because the main effect of a constant β is an overall rescaling of the strength of the fifth force. It is largely degenerate with the average value of $m(a)$, but has no impact on the detectability of time variation of $m(a)$. After marginalizing over β, LSST+ can measure one mass parameter [the average $m(a)$] with an accuracy that is better than 0.01 h/Mpc, or about 5% of the fiducial m_0, and another three parameters, describing more rapid evolution of the mass with time, with accuracy better than 0.02 h/Mpc, or 10% of the fiducial value.

The extrema of the eigenmodes indicate the "sweet spots" in redshift, or epochs at which variations in $m(a)$ are best constrained with LSST+. It is evident from the right panel in Fig. 13, for instance the shape of PC2, that LSST+ is more sensitive to time variations at $z > 1.5$. This is because at higher redshifts there is a larger number of Fourier modes that are still in the linear regime.

V. DISCUSSION AND CONCLUSIONS

Modifications of gravity on cosmological scales can potentially explain the origin of cosmic acceleration. The generalized Brans-Dicke theory, in which there is an additional scalar degree of freedom that mediates a fifth force, is one of the viable MG models that are able to fit observations after the required tuning of model parameters.

In this work, we have investigated the observational constraints on three MG models within the general framework of the GBD theory, namely, the $f(R)$, the symmetron and the dilaton models, using the latest observations of CMB, BAO, weak lensing and galaxy clustering. In all cases, we used observables on linear scales to avoid the complexities of the modeling of nonlinearities and redshift-space distortions.

We find that the ΛCDM model is consistent with all observations. Specifically, we find the constraint on f_{R_0}, the model parameter in the Hu-Sawicki $f(R)$ model, to be $f_{R_0} < 8 \times 10^{-5}$ (95% C.L.) when the sum of neutrino masses is fixed to be 0.06 eV. Since both massive neutrinos and MG models studied in this paper can alter the structure growth in a scale-dependent way, a degeneracy is expected. Therefore we perform another analysis with the neutrino mass varying, and we find that the constraint is diluted to $f_{R_0} < 1.0 \times 10^{-4}$ (95% C.L.). For the symmetron model, the 95% C.L. upper limit is $\xi_\star < 1.8 \times 10^{-3}$ with $\beta_\star$ and $a_\star$ fixed at 1 and 0.25, respectively. For the dilaton model, we find $\xi_0 < 3 \times 10^{-3}$ at 95% C.L. when $\beta_0 = 5$. Tables II and III summarize the current bounds.

We have also performed a forecast for ongoing and upcoming imaging surveys including DES and LSST, and present the results in Sec. IV. A comparison between the current and future constraints on model parameters is shown in Table IV. As one can see, the improvement is significant and, despite the high level of degeneracy, more than one parameter can be constrained simultaneously. In the Hu-Sawicki model, the upper limit of f_{R_0} is reduced by a factor of 6.7 and n can be constrained with $\approx 25\%$ accuracy for $n = 1$. For the dilaton model, current data are unable to constrain ξ_0 if $\beta_0 = 1$. However, we find that LSST+ can simultaneously constrain ξ_0 at $\sim \text{few} \times 10^{-5}$ and measure $\beta_0 \sim 1$ with $\approx 20\%$ accuracy. In the symmetron model, the constraint on $\xi_\star$ is improved by a factor of 3, while simultaneously constraining $a_\star$ and $\beta_\star$ within a few percent. This is compatible with current bounds derived from astrophysical tests, such as the cluster profile [83], galactic dynamics and so on, which requires high-resolution N-body or hydrodynamical simulations [84,85] of the MG models. Additionally, to demonstrate the capabilities of a LSST-like survey, we have presented constraints on the generalized chameleon model in Fig. 12.

Given the power of future surveys, a model-independent analysis will become possible. In this work, we performed a PCA study of $m(a)$, to forecast the maximum number of parameters of the scalaron mass function that can be well determined. We find that a LSST-like survey will be able to measure the average mass parameter with an accuracy of 0.01 h/Mpc and another three parameters quantifying the time variation of $m(a)$ with an accuracy that is better than 0.02 h/Mpc. Finally, we note that future spectroscopic and HI surveys, such as eBOSS and SKA [86,87], will also provide powerful constraints on MG parameters that will be highly complementary to those from a photometric survey like LSST [88].

ACKNOWLEDGMENTS

The research of A. H., A. P., A. Z. and L. P. is supported by the Natural Sciences and Engineering Research Council of Canada (NSERC). A. P. was sponsored in part by the Robert Frazier Memorial Fellowship. A. Z. is supported in part by the Bert Henry Memorial Entrance Scholarship at SFU. G. B. Z. is supported by the Strategic Priority Research Program "The Emergence of Cosmological Structures" of the Chinese Academy of Sciences Grant No. XDB09000000. This research was enabled in part by support provided by WestGrid [89] and Compute Canada [90]. P. B. acknowledges partial support from the European Union FP7 ITN INVISIBLES (Marie Curie Actions, PITN-GA-2011-289442) and from the Agence Nationale de la Recherche under Contract No. ANR 2010 BLANC 0413 01. A. C. D. acknowledges partial support from STFC under Grants No. ST/L000385/1 and No. ST/L000636/1.

[1] A. G. Riess *et al.*, Observational evidence from supernovae for an accelerating universe and a cosmological constant, Astron. J. **116**, 1009 (1998).
[2] S. Perlmutter *et al.*, Measurements of Ω and Λ from 42 high-redshift supernovae, Astrophys. J. **517**, 565 (1999).
[3] C. P. Burgess, The cosmological constant problem: Why it's hard to get dark energy from micro-physics, arXiv:1309.4133.
[4] S. Weinberg, The cosmological constant problem, Rev. Mod. Phys. **61**, 1 (1989).
[5] C. Brans and R. H. Dicke, Mach's principle and a relativistic theory of gravitation, Phys. Rev. **124**, 925 (1961).
[6] J. D. Bekenstein, The relation between physical and gravitational geometry, Phys. Rev. D **48**, 3641 (1993).
[7] M. Zumalacarregui, T. S. Koivisto, D. F. Mota, and P. Ruiz-Lapuente, Disformal scalar fields and the dark sector of the Universe, J. Cosmol. Astropart. Phys. 05 (2010) 038.
[8] H. Y. Ip, J. Sakstein, and F. Schmidt, Solar system constraints on disformal gravity theories, J. Cosmol. Astropart. Phys. 10 (2015) 051.
[9] J. Sakstein and S. Verner, Disformal gravity theories: A Jordan frame analysis, Phys. Rev. D **92**, 123005 (2015).
[10] J. Khoury and A. Weltman, Chameleon cosmology, Phys. Rev. D **69**, 044026 (2004).
[11] P. Brax, C. van de Bruck, A. C. Davis, J. Khoury, and A. Weltman, Detecting dark energy in orbit—The cosmological chameleon, Phys. Rev. D **70**, 123518 (2004).
[12] W. Hu and I. Sawicki, Models of f(R) cosmic acceleration that evade solar-system tests, Phys. Rev. D **76**, 064004 (2007).
[13] P. Brax, C. van de Bruck, A. C. Davis, and D. J. Shaw, f(R) gravity and chameleon theories, Phys. Rev. D **78**, 104021 (2008).
[14] P. Brax, C. van de Bruck, A. C. Davis, and D. Shaw, The dilaton and modified gravity, Phys. Rev. D **82**, 063519 (2010).
[15] K. Hinterbichler and J. Khoury, Symmetron Fields: Screening Long-Range Forces Through Local Symmetry Restoration, Phys. Rev. Lett. **104**, 231301 (2010).
[16] T. Damour and A. M. Polyakov, The string dilaton and a least coupling principle, Nucl. Phys. **B423**, 532 (1994).
[17] P. Brax, A.-C. Davis, and B. Li, Modified gravity tomography, Phys. Lett. B **715**, 38 (2012).
[18] P. Brax, A.-C. Davis, B. Li, and H. A. Winther, A unified description of screened modified gravity, Phys. Rev. D **86**, 044015 (2012).
[19] M. Ishak, A. Upadhye, and D. N. Spergel, Probing cosmic acceleration beyond the equation of state: Distinguishing

between dark energy and modified gravity models, Phys. Rev. D **74**, 043513 (2006).
[20] E. V. Linder, Cosmic growth history and expansion history, Phys. Rev. D **72**, 043529 (2005).
[21] M. Kunz and D. Sapone, Dark Energy versus Modified Gravity, Phys. Rev. Lett. **98**, 121301 (2007).
[22] P. Zhang, M. Liguori, R. Bean, and S. Dodelson, Probing Gravity at Cosmological Scales by Measurements which Test the Relationship between Gravitational Lensing and Matter Overdensity, Phys. Rev. Lett. **99**, 141302 (2007).
[23] L. Amendola, M. Kunz, and D. Sapone, Measuring the dark side (with weak lensing), J. Cosmol. Astropart. Phys. 04 (2008) 013.
[24] Y. S. Song and K. Koyama, Consistency test of general relativity from large scale structure of the Universe, J. Cosmol. Astropart. Phys. 01 (2009) 048.
[25] G. B. Zhao, L. Pogosian, A. Silvestri, and J. Zylberberg, Searching for modified growth patterns with tomographic surveys, Phys. Rev. D **79**, 083513 (2009).
[26] Y. S. Song and O. Dore, A step towards testing general relativity using weak gravitational lensing and redshift surveys, J. Cosmol. Astropart. Phys. 03 (2009) 025.
[27] G. B. Zhao, L. Pogosian, A. Silvestri, and J. Zylberberg, Cosmological Tests of General Relativity with Future Tomographic Surveys, Phys. Rev. Lett. **103**, 241301 (2009).
[28] S. F. Daniel, E. V. Linder, T. L. Smith, R. R. Caldwell, A. Cooray, A. Leauthaud, and L. Lombriser, Testing general relativity with current cosmological data, Phys. Rev. D **81**, 123508 (2010).
[29] G. B. Zhao, T. Giannantonio, L. Pogosian, A. Silvestri, D. J. Bacon, K. Koyama, R. C. Nichol, and Y. S. Song, Probing modifications of General Relativity using current cosmological observations, Phys. Rev. D **81**, 103510 (2010).
[30] L. Pogosian, A. Silvestri, K. Koyama, and G.-B. Zhao, How to optimally parametrize deviations from GR in the evolution of cosmological perturbations, Phys. Rev. D **81**, 104023 (2010).
[31] C. Shapiro, S. Dodelson, B. Hoyle, L. Samushia, and B. Flaugher, Will multiple probes of dark energy find modified gravity?, Phys. Rev. D **82**, 043520 (2010).
[32] S. F. Daniel and E. V. Linder, Confronting general relativity with further cosmological data, Phys. Rev. D **82**, 103523 (2010).
[33] Y. S. Song, G. B. Zhao, D. Bacon, K. Koyama, R. C. Nichol, and L. Pogosian, Complementarity of weak lensing and peculiar velocity measurements in testing general relativity, Phys. Rev. D **84**, 083523 (2011).
[34] A. Hojjati, L. Pogosian, and G.-B. Zhao, Testing gravity with CAMB and CosmoMC, J. Cosmol. Astropart. Phys. 08 (2011) 005.
[35] A. Hojjati, G.-B. Zhao, L. Pogosian, A. Silvestri, R. Crittenden, and K. Koyama, Cosmological tests of general relativity: A principal component analysis, Phys. Rev. D **85**, 043508 (2012).
[36] A. Hojjati, Degeneracies in parametrized modified gravity models, J. Cosmol. Astropart. Phys. 01 (2013) 009.
[37] A. Hojjati, L. Pogosian, A. Silvestri, and S. Talbot, Practical solutions for perturbed f(R) gravity, Phys. Rev. D **86**, 123503 (2012).
[38] S. F. Daniel and E. V. Linder, Constraining cosmic expansion and gravity with galaxy redshift surveys, J. Cosmol. Astropart. Phys. 02 (2013) 007.
[39] F. Simpson *et al.*, CFHTLenS: Testing the laws of gravity with tomographic weak lensing and redshift space distortions, Mon. Not. R. Astron. Soc. **429**, 2249 (2013).
[40] A. Silvestri, L. Pogosian, and R. V. Buniy, Practical approach to cosmological perturbations in modified gravity, Phys. Rev. D **87**, 104015 (2013).
[41] A. Hojjati, L. Pogosian, A. Silvestri, and G. B. Zhao, Observable physical modes of modified gravity, Phys. Rev. D **89**, 083505 (2014).
[42] B. Hu, M. Liguori, N. Bartolo, and S. Matarrese, Parametrized modified gravity constraints after Planck, Phys. Rev. D **88**, 123514 (2013).
[43] J. Dossett, B. Hu, and D. Parkinson, Constraining models of f(R) gravity with Planck and WiggleZ power spectrum data, J. Cosmol. Astropart. Phys. 03 (2014) 046.
[44] P. A. R. Ade *et al.* (Planck Collaboration), Planck 2015 results. XIV. Dark energy and modified gravity, arXiv:1502.01590.
[45] B. Jain, V. Vikram, and J. Sakstein, Astrophysical tests of modified gravity: Constraints from distance indicators in the nearby Universe, Astrophys. J. **779**, 39 (2013).
[46] V. Vikram, A. Cabr, B. Jain, and J. T. VanderPlas, Astrophysical tests of modified gravity: The morphology and kinematics of dwarf galaxies, J. Cosmol. Astropart. Phys. 08 (2013) 020.
[47] J. Sakstein, B. Jain, and V. Vikram, Detecting modified gravity in the stars, Int. J. Mod. Phys. D **23**, 1442002 (2014).
[48] J. Bel, P. Brax, C. Marinoni, and P. Valageas, Cosmological tests of modified gravity: Constraints on $F(R)$ theories from the galaxy clustering ratio, Phys. Rev. D **91**, 103503 (2015).
[49] P. Brax, Environmental variation of constants in screened modified theories of gravity, Phys. Rev. D **90**, 023505 (2014).
[50] http://www.lsst.org.
[51] http://www.euclid-ec.org.
[52] C. Schimd, J. P. Uzan, and A. Riazuelo, Weak lensing in scalar-tensor theories of gravity, Phys. Rev. D **71**, 083512 (2005).
[53] http://www.camb.info.
[54] http://www.sfu.ca/~aha25/MGCAMB.html.
[55] P. Brax and P. Valageas, Impact on the power spectrum of screening in modified gravity scenarios, Phys. Rev. D **88**, 023527 (2013).
[56] C. Llinares and D. Mota, Releasing Scalar Fields: Cosmological Simulations of Scalar-Tensor Theories for Gravity Beyond the Static Approximation, Phys. Rev. Lett. **110**, 161101 (2013).
[57] J. Gleyzes, D. Langlois, F. Piazza, and F. Vernizzi, Essential building blocks of dark energy, J. Cosmol. Astropart. Phys. 08 (2013) 025.
[58] J. Bloomfield, A simplified approach to general scalar-tensor theories, J. Cosmol. Astropart. Phys. 12 (2013) 044.
[59] B. Hu, M. Raveri, N. Frusciante, and A. Silvestri, Effective field theory of cosmic acceleration: An implementation in CAMB, Phys. Rev. D **89**, 103530 (2014).

[60] M. Raveri, B. Hu, N. Frusciante, and A. Silvestri, Effective field theory of cosmic acceleration: Constraining dark energy with CMB data, Phys. Rev. D **90**, 043513 (2014).
[61] A. G. Riess *et al.*, Observational evidence from supernovae for an accelerating universe and a cosmological constant, The Astronomical Journal **116**, 1009 (1998).
[62] S. M. Carroll, V. Duvvuri, M. Trodden, and M. S. Turner, Is cosmic speed-up due to new gravitational physics?, Phys. Rev. D **70**, 043528 (2004).
[63] S. A. Appleby and R. A. Battye, Do consistent $F(R)$ models mimic general relativity plus Λ?, Phys. Lett. B **654**, 7 (2007).
[64] A. A. Starobinsky, Disappearing cosmological constant in f (R) gravity, JETP Lett. **86**, 157 (2007).
[65] P. Brax, A. C. Davis, B. Li, H. A. Winther, and G. B. Zhao, Systematic simulations of modified gravity: Chameleon models, J. Cosmol. Astropart. Phys. 04 (2013) 029.
[66] http://cosmologist.info/cosmomc/.
[67] P. A. R. Ade *et al.* (Planck Collaboration), Planck 2015 results. XIII. Cosmological parameters, arXiv:1502.01589.
[68] P. A. R. Ade *et al.* (Planck Collaboration), Planck 2015 results. XV. Gravitational lensing, arXiv:1502.01591.
[69] P. A. R. Ade *et al.* (Planck Collaboration), Planck 2013 results. XVI. Cosmological parameters, Astron. Astrophys. **571**, A16 (2014).
[70] G. E. Addison, Y. Huang, D. J. Watts, C. L. Bennett, M. Halpern, G. Hinshaw, and J. L. Weiland, Quantifying discordance in the 2015 Planck CMB spectrum, arXiv:1511.00055.
[71] F. Beutler, C. Blake, M. Colless, D. H. Jones, L. Staveley-Smith, L. Campbell, L. Q. Parker, W. Saunders, and F. Watson, The 6dF Galaxy Survey: Baryon acoustic oscillations and the local Hubble constant, Mon. Not. R. Astron. Soc. **416**, 3017 (2011).
[72] A. J. Ross, L. Samushia, C. Howlett, W. J. Percival, A. Burden, and M. Manera, The clustering of the SDSS DR7 main Galaxy sample I. A 4 per cent distance measure at $z = 0.15$, Mon. Not. R. Astron. Soc. **449**, 835 (2015).
[73] L. Anderson *et al.* (BOSS Collaboration), The clustering of galaxies in the SDSS-III Baryon Oscillation Spectroscopic Survey: Baryon acoustic oscillations in the Data Releases 10 and 11 Galaxy samples, Mon. Not. R. Astron. Soc. **441**, 24 (2014).
[74] M. Tegmark *et al.* (SDSS Collaboration), Cosmological constraints from the SDSS luminous red galaxies, Phys. Rev. D **74**, 123507 (2006).
[75] G. B. Zhao *et al.*, The clustering of galaxies in the SDSS-III Baryon Oscillation Spectroscopic Survey: Weighing the neutrino mass using the galaxy power spectrum of the CMASS sample, Mon. Not. R. Astron. Soc. **436**, 2038 (2013).
[76] M. Kilbinger, L. Fu, C. Heymans *et al.*, CFHTLenS: Combined probe cosmological model comparison using 2D weak gravitational lensing, Mon. Not. R. Astron. Soc. **430**, 2200 (2013).
[77] Z. Ivezic, J. A. Tyson *et al.* (LSST Collaboration), LSST: From science drivers to reference design and anticipated data, arXiv:0805.2366.
[78] http://www.darkenergysurvey.org/.
[79] http://www.camb.info/sources/.
[80] M. Tegmark, A. Taylor, and A. Heavens, Karhunen-Loeve eigenvalue problems in cosmology: How should we tackle large data sets?, Astrophys. J. **480**, 22 (1997).
[81] D. Huterer and G. Starkman, Parameterization of Dark-Energy Properties: A Principal-Component Approach, Phys. Rev. Lett. **90**, 031301 (2003).
[82] R. G. Crittenden, L. Pogosian, and G. B. Zhao, Investigating dark energy experiments with principal components, J. Cosmol. Astropart. Phys. 12 (2009) 025.
[83] H. Wilcox *et al.*, The XMM Cluster Survey: Testing chameleon gravity using the profiles of clusters, Mon. Not. R. Astron. Soc. **452**, 1171 (2015).
[84] P. Brax, A. C. Davis, B. Li, H. A. Winther, and G. B. Zhao, Systematic simulations of modified gravity: Symmetron and dilaton models, J. Cosmol. Astropart. Phys. 10 (2012) 002.
[85] P. Brax, A. C. Davis, B. Li, H. A. Winther, and G. B. Zhao, Systematic simulations of modified gravity: Chameleon models, J. Cosmol. Astropart. Phys. 04 (2013) 029.
[86] G. B. Zhao *et al.*, The extended Baryon Oscillation Spectroscopic Survey (eBOSS): A cosmological forecast, arXiv:1510.08216.
[87] G. B. Zhao, D. Bacon, R. Maartens, M. Santos, and A. Raccanelli, Model-independent constraints on dark energy and modified gravity with the SKA, arXiv:1501.03840.
[88] D. Bacon *et al.*, Synergy between the Large Synoptic Survey Telescope and the Square Kilometre Array, *Proc. Sci.*, AASKA 14 (2015) 145 [arXiv:1501.03977].
[89] http://www.westgrid.ca.
[90] http://www.computecanada.ca.